



# C57BL/6 and Swiss Webster Mice Display Differences in Mobility, Gliosis, Microcavity Formation and Lesion Volume After Severe Spinal Cord Injury

Harun Najib Noristani<sup>1,2\*</sup>, Laetitia They<sup>2</sup> and Florence Evelyne Perrin<sup>1,2</sup>

<sup>1</sup>INSERM U1198, University of Montpellier, EPHE, Montpellier, France, <sup>2</sup>INSERM U1051, Montpellier, France

## OPEN ACCESS

### Edited by:

Antonio J. Herrera,  
Universidad de Sevilla, Spain

### Reviewed by:

Liuqing Yang,  
Johns Hopkins Medicine,  
United States  
Melissa R. Andrews,  
University of Southampton,  
United Kingdom

### \*Correspondence:

Harun N. Noristani  
harun.noristani@ibn-lab.com

**Received:** 12 April 2018

**Accepted:** 01 June 2018

**Published:** 21 June 2018

### Citation:

Noristani HN, They L and Perrin FE (2018) C57BL/6 and Swiss Webster Mice Display Differences in Mobility, Gliosis, Microcavity Formation and Lesion Volume After Severe Spinal Cord Injury. *Front. Cell. Neurosci.* 12:173. doi: 10.3389/fncel.2018.00173

Spinal cord injuries (SCI) are neuropathologies causing enormous physical and emotional anguish as well as irreversibly disabilities with great socio/economic burdens to our society. The availability of multiple mouse strains is important for studying the underlying pathophysiological response after SCI. Although strain differences have been shown to directly affect spontaneous functional recovery following incomplete SCI, its influence after complete lesion of the spinal cord is unclear. To study the influence of mouse strain on recovery after severe SCI, we first carried out behavioral analyses up to 6 weeks following complete transection of the spinal cord in mice with two different genetic backgrounds namely, C57BL/6 and Swiss Webster. Using immunohistochemistry, we then analyzed glial cell reactivity not only at different time-points after injury but also at different distances from the lesion epicenter. Behavioral assessments using CatWalk™ and open field analyses revealed increased mobility (measured using average speed) and differential forelimb gross sensory response in Swiss Webster compared to C57BL/6 mice after complete transection of the spinal cord. Comprehensive histological assessment revealed elevated microglia/macrophage reactivity and a moderate increase in astrogliosis in Swiss Webster that was associated with reduced microcavity formation and reduced lesion volume after spinal cord transection compared to C57BL/6 mice. Our results thus suggest that increased mobility correlates with enhanced gliosis and better tissue protection after complete transection of the spinal cord.

**Keywords:** spinal cord injury, glial cells, microcavity, protection, mobility

## INTRODUCTION

Spinal cord injury (SCI) is a distressing neuropathology that affects over 2.5 million people worldwide with an annual incidence of 40–60 per million populations (van den Berg et al., 2010). Depending on the anatomical level and lesion severity, clinical symptoms related with SCI range from minor sensory/motor impairments to complete quadriplegia. Following the initial mechanical damages to the spinal cord there are a series of secondary events including neuroinflammation, oedema, microcavity formation and gliosis that altogether govern tissue re-organization and

functional impairment after SCI (Hausmann, 2003). Microglia and astrocytes are the two glial cell populations predominantly involved in scar formation.

To uncover the underlying pathophysiology of SCI several animal models have been developed including spinal cord compression, contusion, ischemia, hemisection and complete transection (Lee and Lee, 2013). Recent advances in surgical devices have helped to generate reliable models of SCI in animals with minimal inter-individual variations in lesion severity (Basso et al., 1996b; Onifer et al., 2007). While complete transection is considered as the most deleterious SCI model, it permits to avoid the inter-individual variations in lesion severity (M'Dahoma et al., 2014). In addition, as complete transection model is very reproducible, it allows usage of a smaller number of animals. Furthermore, complete transection is the most rigorous model to study axon regeneration because the two segments of the spinal cord are totally separated with no spared axons (Lee and Lee, 2013). Indeed, complete transection model has been extensively used to study functional recovery, although majority of reports have focused on rats (Basso et al., 1996a; Antri et al., 2005; Onifer et al., 2007; M'Dahoma et al., 2014).

Multiple mouse strains with different transgenic backgrounds are now available to study the underlying pathophysiological mechanisms after SCI. However, there are inherent differences in mouse strains that affects neuroinflammation, tissue preservation and spontaneous functional recovery following incomplete SCI (Basso et al., 2006; Kigerl et al., 2006; Lapointe et al., 2006; Kerr and David, 2007). Previously, Ma et al. (2004) reported reduced inflammation in 129X1-SvJ associated with increase regeneration compared to C57BL/6 mice strain after contusion SCI, although the authors found no difference in functional recovery between the two strains of mice. Subsequently, Kigerl et al. (2006) reported increased microglial/macrophage activation in C57BL/6 after contusion SCI compared to C57BL/10, BALB/c and B10.PL mouse strains, although all four groups displayed similar changes in lesion volume.

To study the specific role of glial cells after SCI, we have recently used transgenic mice that express enhanced green fluorescence protein (eGFP) either in astrocytes (Aldh1l1-EGFP) or in microglia/monocytes (CX3CR1<sup>+eGFP</sup>; Noristani and Perrin, 2016; Noristani et al., 2016, 2017b). Aldh1l1-EGFP are maintained in Swiss Webster, whereas CX3CR1<sup>+eGFP</sup> mice have C57BL/6 genetic background that may influence spontaneous functional recovery and tissue histopathology after spinal cord transection.

Here, we have carried out detailed behavioral and histological assessments after complete transection of the spinal cord in mice with two different genetic background namely, Swiss Webster and C57BL/6, respectively. Using CatWalk™ and open field analyses we observed increased mobility after complete transection in Swiss Webster compared to C57BL/6 mice that was associated with increased gliosis, better tissue preservation and reduced lesion volume. Our findings highlight the positive correlation between increased mobility, enhanced gliosis and better tissue protection after complete transection of the spinal cord.

## MATERIALS AND METHODS

### Animals

All experiments followed the French and EU regulations (EU/Directive/2010/63 of the European Parliament and Council). All experimental protocols were approved by the “Ministère de l'Éducation Nationale, de l'Enseignement Supérieur et de la Recherche” and the regional ethic committee for animal experimentation (CEEA-Languedoc Roussillon, authorization number: 34,118), France. All efforts were made to minimize animal number and their suffering. We used, transgenic mice strains expressing selectively enhanced green fluorescent protein (eGFP) either in astrocytes (Aldh1l1-EGFP)OFC789Gsat/Mmucd, Mutant Mouse Regional Resource Centre) (Cahoy et al., 2008) or in microglia (CX3CR1, obtained from Dr. Dan Littman, Howard Hughes Medical Institute, Skirball Institute, NYU Medical Centre, NY, USA). These mice are maintained in different genetic backgrounds namely, Swiss Webster for Aldh1l1 and C57BL/6 for CX3CR1 mice, respectively. Heterozygous CX3CR1<sup>+eGFP</sup> and wild type (WT) Aldh1l1 (not expressing eGFP) were used in the current study that were confirmed by polymerase chain reaction (PCR). Previous studies have shown that CX3CR1<sup>+eGFP</sup> display similar microglia phenotype to IBA1-EGFP transgenic mice (Hirasawa et al., 2005). Transcriptomic analysis revealed less than 0.5% differences in deregulated genes between WT and CX3CR1<sup>+eGFP</sup> microglia (Solga et al., 2015). More recently, Hirbec et al. (2018) also reported no difference in deregulated genes between WT and CX3CR1<sup>+eGFP</sup> microglia after lipopolysaccharide challenge. Altogether, these studies suggest that eGFP expression in CX3CR1<sup>+eGFP</sup> microglia do not affect their phenotype under both physiological and inflammatory condition. We have also carried out immunohistochemical analysis for GFAP and IBA1 expression following injury in WT and Aldh1l1-EGFP littermates and observed no difference in glial response (data not shown). We will from now refer in the text to mice strains as Swiss Webster and C57BL/6. All mice were housed in controlled conditions (hygrometry, temperature and 12 h light/dark cycle).

### Spinal Cord Injury and Postoperative Cares

Adult female mice (12 weeks) were anesthetized and received inhaled isoflurane gas (1.5%); a thoracic 9 (T9) laminectomy was performed and complete transection was carried out under the microscope (Leica M80, Nanterre, France) using a micro-scalpel (10315-12, Fine Science Tools, Heidelberg, Germany), as described previously (Noristani et al., 2015, 2016, 2017a,b). **Table 1** summarizes the number of animals used for behavioral analysis and histological assessment at multiple time-points after injury. Lesions were done at T9 vertebra level to obtain complete paraplegia whilst preserving full respiratory function. Bladders were emptied manually twice daily throughout the study period. Bodyweight was measured before surgery and continued daily till 6 weeks post-lesion.

**TABLE 1** | Summary of the number of animals used for behavioral analysis and histological assessment at multiple time-points after complete transection of the spinal cord in both strains of mice.

Strain	Behavioral analysis		Histological analysis				Total 79	
	Un-injured	Injured	Un-injured	1 week	2 weeks	4 weeks		6 weeks
Swiss Webster	5	5	5	6	6	6	5	38
C57BL/6	6	8	5	6	4	6	6	41

## Behavioral Analysis

Mice underwent behavioral assessments (CatWalk™ and open field) at 7 and 1 days before injury followed by 24 and 72 h and then once a week up to 6 weeks after lesion compared to that of non-injured (NI) control.

### CatWalk™

CatWalk™ permits the dynamic walking patterns analysis (Noldus, Wageningen, Netherlands). Several parameters (total speed, print area and max contact) were analyzed. We used the CatWalk™ associated with CatMerge (InnovationNet, France), as previously described (Gerber et al., 2012). Eight to ten runs per animal were performed at each time-point with a minimum of five runs at the same speed; at least 3-full step sequence patterns per run were recorded. To avoid bias due to stress, we placed all mice on the CatWalk™ plate for 20 min 7 days prior to the first recording session.

### Open Field Activity

Spontaneous locomotor activity was monitored using open field test (**Supplementary Figure S1B**). Mice were placed in an empty test arena (45 × 45 cm box) and their movements were automatically recorded by a camera. Average speed was calculated using EthoTrack (InnovationNet, Tiranges, France). In addition, we also evaluated modification in forelimb gross sensory response after injury using sandpapers, as previously described (Wetzel et al., 2007). The open field floor was divided into four areas composed of four different granularities of sandpapers with mean grain size of 100, 200, 270 and 425 /μm (**Supplementary Figure S1B**). Considering the mean grain size in each of the four sandpapers, the open field was divided into smooth (mean grain size 100/μm, 1 compartment) and rough (mean grain size >200/μm, three compartments). Times spent on the smooth and rough sandpapers were analyzed automatically using EthoTrack (InnovationNet, Tiranges, France). Mice were placed on individual sandpapers and positioned on the same surface area and orientation. Each analysis session involved 20 min of recording (10 min on plain ground for motor activity followed by 10 min on sandpaper grounds) preceded by 4 min without recording. All mice were placed in the open field for a period of 30 min 7 days prior to the first recording session. To assess SCI-induced anxiety in mouse behavior, the open field data were analyzed by dividing the arena into centralized (22.5 × 22.5 cm) area and the remaining outside zone. Time spent on the centralized and outside zones were measured throughout 6 weeks after injury.

## Primary Antibodies for Immunological Staining

Primary antibodies used included polyclonal rabbit anti GFAP (1:1000; Z0334; Dako, Glostrup, Denmark), mouse anti vimentin (1:500; V2258-2ML; Sigma Aldrich, St. Louis, USA) and rabbit anti-IBA1 (1:1000; 019-19741; Wako Pure Chemical Industries, Osaka, Japan).

## Immunohistochemistry

Mice were anesthetized with tribromoethanol (500 mg/kg, i.p) and perfused intracardially with 0.1 M phosphate base saline (PBS) followed by 4% paraformaldehyde (PFA, Sigma Aldrich, St. Louis, USA). Spinal cords were removed and post-fixed for additional 2 h in 4% PFA, cryoprotected in 30% sucrose, included in Tissue Teck (Sakura, Alphen aan den Rijn, Netherlands), frozen and kept at -20°C until processing. Spinal cords were cut longitudinally (22 μm) using a cryostat (Microm, Heidelberg, Germany) and were collected on super frost plus slides. For fluorescence immunohistochemistry, slides were washed in 0.1 M PBS and incubated for 20 min in 20 mM lysine (pH 7.2). Sections were then permeabilized and blocked for 1 h with 0.1 M PBS containing 1% bovine serum albumin (BSA, Sigma Aldrich, St. Louis, USA) and 0.1% Triton X-100 (Fisher Scientific, Illkirch, France) followed by incubation in primary antibody for 48 h at 4°C. Slides were then washed in 0.1 M PBS and were placed in corresponding secondary antibodies conjugated to Alexa 488, 594 or 633 (Vector Laboratories, Peterborough, United Kingdom and Millipore Bioscience Research Re-agents, Fontenay sous Bois, France). Sections were cover slipped using fluorescence mounting medium (Dako, Glostrup, Denmark). Morphometric fluorescent photographs were obtained and analyzed using NanoZoomer RS slide scanner (NanoZoomer Digital Pathology System and NDP view software, Hamamatsu, Japan). In addition, we also used laser scanning inverted (Leica SP5, Mannheim, Germany) and (Zeiss five Live Duo, Oberkochen, Germany) confocal microscopy. Four time-points after injury were analyzed at histological levels namely, 1, 2, 4 and 6 weeks after lesion (**Table 1**). All sections used for immunofluorescence analysis were selected in random. Sections were number coded to ensure blind analyses (both strain and time post-lesion) throughout the experiment. The codes were not revealed until the end of the experiment.

## Immunohistochemistry Analysis

For measurement of astrogliosis and microglia/macrophage response three to five sections per mouse were analyzed per time-points. Astrogliosis was assessed using glial fibrillary

acidic protein (GFAP) and vimentin staining. For microgliosis we used ionized calcium-binding adapter molecule 1 (IBA1) immunostaining. Five different zones at specific distances away from the edge of the astroglia scar border across the entire diameter of each longitudinal section rostral and caudal to the lesion sites were analyzed (**Supplementary Figure S1A**). These zones included (Z1) 0–250  $\mu\text{m}$  immediately adjacent to the lesion site, (Z2) between 250–500  $\mu\text{m}$  away, (Z3) 1000–1250  $\mu\text{m}$  away, (Z4) 2000–2250  $\mu\text{m}$  away and (Z5) 4000–4250  $\mu\text{m}$  from the lesion site. Zones across the spinal cord sections were traced in at least  $n = 4$  mice per group (4–7 mice per group) using a computer-driven stage. In NI mice, we analyzed optical density and area fraction in the equivalent anatomical levels of the spinal cord (**Supplementary Figure S1A**).

### Relative Optical Density

To determine glial reactivity, the mean optical density was measured at different distances and time-points after SCI. Optical density is a sensitive and reliable approach to measure expression level of a given signal and to detect changes caused by experimental conditions. Immunofluorescence labelled spinal cord sections were scanned using Nanozoomer RS slide scanner that uses constant exposure time to obtain fluorescence-labeled photographs (NanoZoomer Digital Pathology System and NDP view software, Hamamatsu, Japan). To further avoid potential variation in staining intensity between different slides or animals, for each of the given antibody, we carried out immunostaining of all animals in parallel. The different zones used for optical density analysis were identified using Nanozoomer software and digital images were exported as RGB using identical exposure settings. Optical density quantification was performed using ImageJ software (NIH, USA). Optical density measures were determined in randomly selected longitudinal section with clearly visible lesion site from each mouse spinal cord. To measure staining density in different zones, optical density measures included the individual zones both rostral and caudal to the lesion site in each section.

### Area Fraction

To analyze the proportional area occupied by glial cells at different distances to the lesion site, we carried out area fraction analysis using ImageJ software (NIH, USA). All sections used for optical density measurement also underwent area fraction analysis. Threshold was adjusted according to NI control and this was kept constant for all images analyzed. Area fraction was analyzed individually in all five mentioned zones both rostral and caudal to the lesion site.

### Quantification of Microcavities and Lesion Volume

Microcavities are devoid of reactive astrocytes and are frequently observed in SCI patients and animal models. To identify microcavities, longitudinal sections were stained using GFAP antibody, as described previously (Thuret et al., 2012). Microcavities were measured as the area fraction in Z1–Z5 of tissues without GFAP staining as compared to total surface area, both rostral and caudal to the lesion site. Lesion volume

was also measured in GFAP-stained longitudinal sections, as previously described (Nelissen et al., 2014; Gadani et al., 2015). Microcavities and lesion volume were measured in over five longitudinally cut sections per mouse with 110  $\mu\text{m}$  intervals throughout the spinal cord. The area with no GFAP was selected as lesion area and was measured in each animal of the group ( $n = 4$ –8). Lesion area in each section was quantified using ImageJ and lesion volume was quantified by multiplying the measured surface area by the section thickness. Measured volumes were then summed for the final estimation of lesion volume in cubic millimeters.

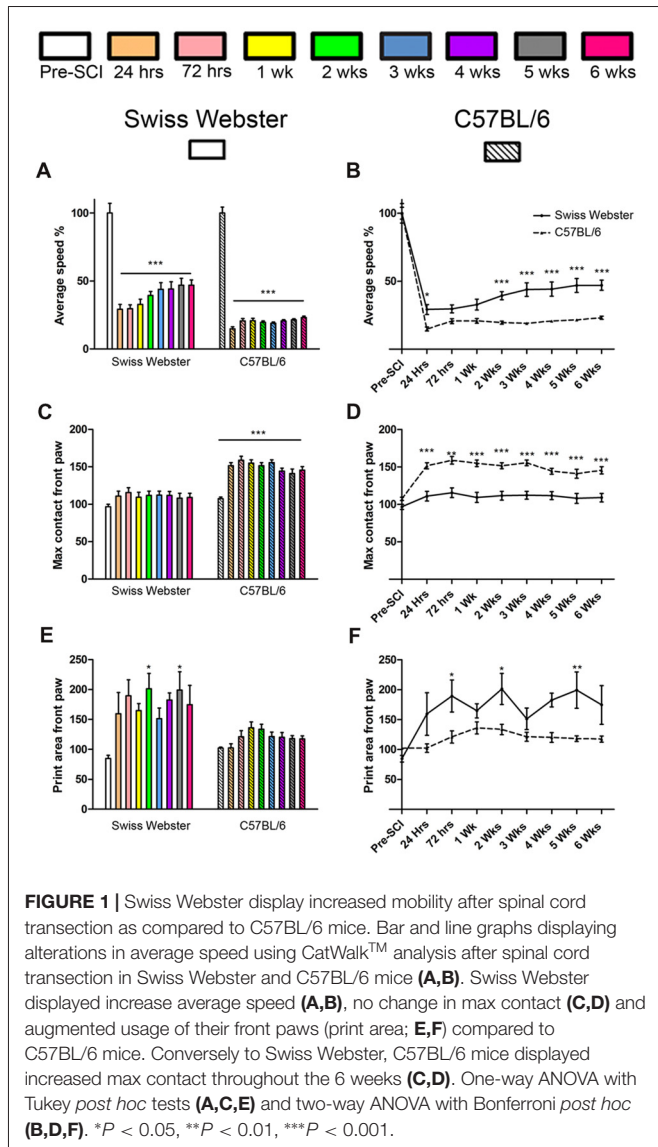
### Statistical Analysis

Two-way ANOVA with Bonferroni *post hoc* tests were used for multiple comparisons in the two strains of mice (behavior, GFAP, IBA1 and microcavities). One-way ANOVA with Tukey *post hoc* tests were used for multiple comparisons (staining intensities at different distance to injury vs. NI control) for each given mouse strain. To directly compare the two strains, we first verified that the basal level for a given parameter (basal behavioral parameter, protein intensity and microcavities percentage) in NI animals were similar in both strains of mice. GFAP expression and cavities were similar in both strains of mice prior to injury. For behavioral parameters and IBA1 intensity, as basal expression levels were different between the two strains in un-injured controls, we normalized the data for each given strain to the value obtained before injury (behavior parameters) or to NI controls (IBA1 intensity), respectively. Un-paired *t*-tests were used to compare differences in lesion volume. Significance was accepted at  $p \leq 0.05$ . All data were analyzed using GraphPad Prism 4.0 (GraphPad Software, Inc., CA, USA). Data are shown as the mean  $\pm$  standard error of the mean (SEM).

## RESULTS

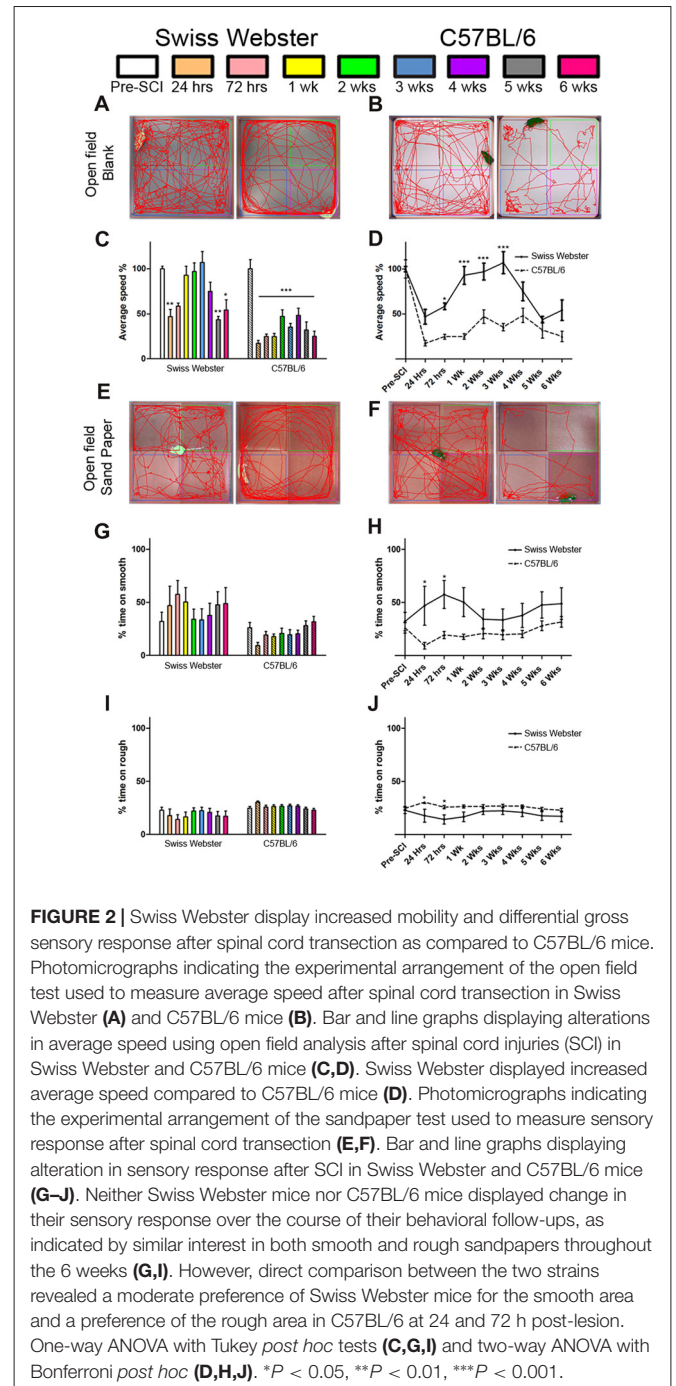
### Swiss Webster Show Increased Mobility Than C57BL/6 Mice After Complete Transection

To determine strain-dependent differences in spontaneous functional recovery post-injury, we carried out detailed behavioral assessments using CatWalk™ and open field analyses. Analysis of average speed using CatWalk™ revealed pronounced decrease in mobility after injury in both strains of mice at 24 h post-lesion reaching 29% in the case of Swiss Webster and only 15% for C57BL/6 mice compared to before surgery (**Figures 1A,B**). Swiss Webster mice displayed a steady increase in their average speed overtime reaching over 47% by 5 weeks post-lesion compared to before injury (**Figures 1A,B**). C57BL/6 mice, on the other hand, did not display increased speed overtime, they indeed remained at 23% at 6 weeks post-lesion compared to before injury (**Figures 1A,B**). Thus, Swiss Webster mice showed a less affected speed and a better recovery after injury as compared to C57BL/6 mice throughout the 6 weeks period after spinal cord transection (**Figures 1A,B**). Increased mobility in Swiss Webster mice after complete transection was also evident using max contact parameter of



the CatWalk™, which is the time a paw contacts the glass plate. Indeed, Swiss Webster did not show an increase in max contact of their front paw whilst C57BL/6 mice displayed an increase in max area from 24 h following injury that remain stable throughout 6 weeks post-injury (Figures 1C,D). Increased speed in Swiss Webster mice was due to greater function of their front paws as indicated by an increase in print surface area compared to C57BL/6 mice (Figures 1E,F). No movement of the hind paws was observed in either Swiss Webster or C57BL/6 mice throughout 6 weeks analyses after spinal cord transection (Supplementary Figures S1C,D). Following complete transection of the spinal cord we only observed dragging of the hind paws. No plantar placement of the hind paws was evident in either strains of mice throughout 6 weeks after lesion.

Open field analysis further confirmed increased mobility in Swiss Webster than C57BL/6 mice after spinal cord transection (Figure 2). Swiss Webster mice displayed significant decrease



in their average speed up to 72 h post-lesion followed by a transient increase in speed between 1–3 weeks post-lesion (Figures 2A,C). Conversely, C57BL/6 mice displayed constant reduced speed throughout 6 weeks after injury compared to before surgery (Figures 2B,C). Direct comparison between the two strains of mice using open field showed significant increase in speed from 72 h until 3 weeks after SCI in Swiss Webster compared to C57BL/6 mice (Figure 2D). To determine whether the increased mobility reflects differences in anxiety behavior, we analyzed the open field recordings for anxiety (Supplementary

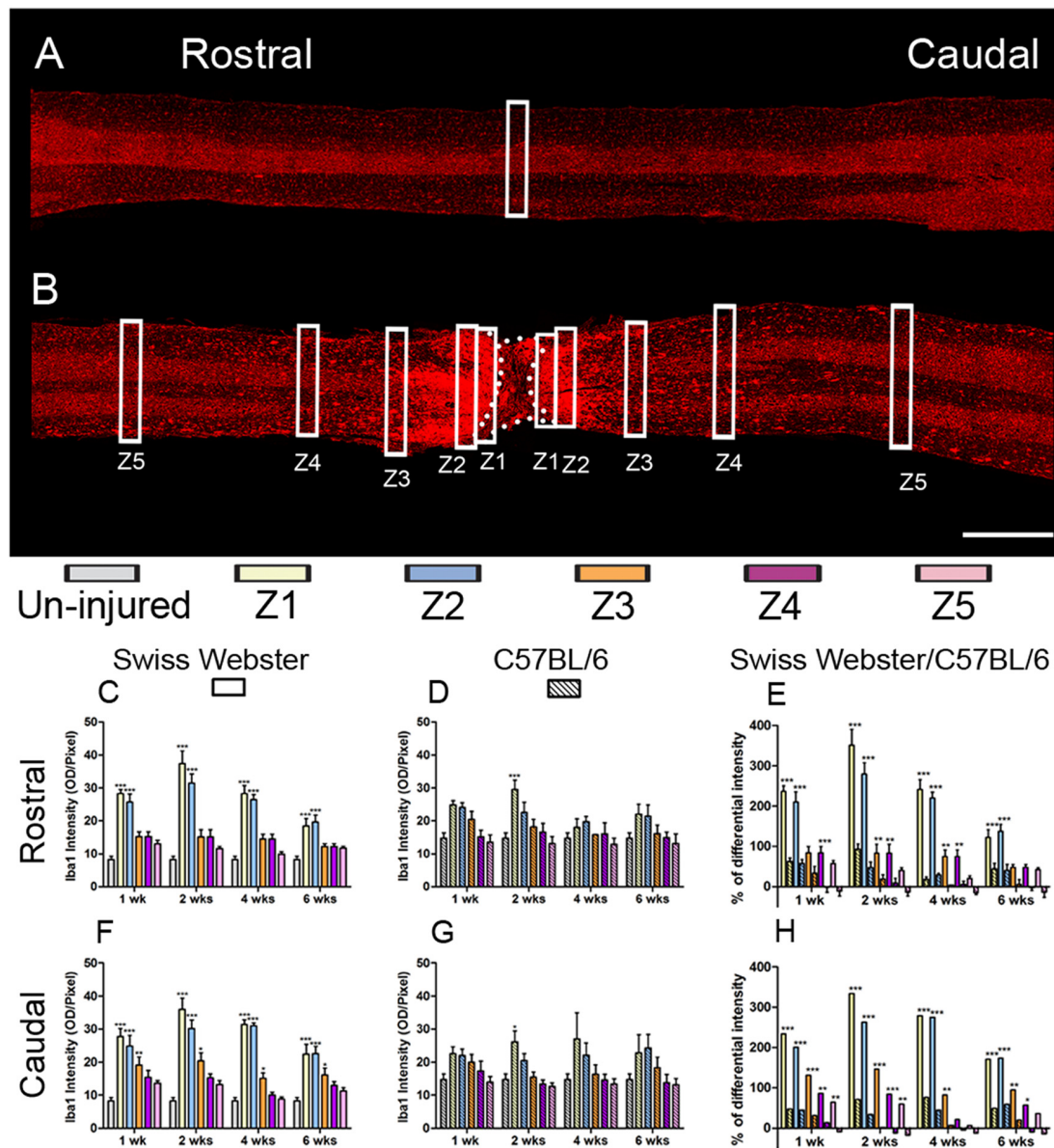


**FIGURE 3 |** Increased microglia/macrophage response in Swiss Webster compared to C57BL/6 mice after severe SCI. Confocal photomicrographs indicating IBA1 staining of longitudinal spinal cord sections in the non-injured (NI) control and spinal cord transected mice (A,B). Bar graphs indicating quantitative analysis of IBA1 immunoreactivity along the five zones rostral and caudal to the lesion site in Swiss Webster mice (C,F) and C57BL/6 mice (D,G). Direct comparisons following normalization revealed that Swiss Webster displayed increased IBA1 immunoreactivity compared to C57BL/6 mice after spinal cord transection (E,H). Scale bars (A,B): 1 mm. One-way ANOVA with Tukey *post hoc* tests (C,D,F,G) and two-way ANOVA with Bonferroni *post hoc* (E,H). \* $P < 0.05$ , \*\* $P < 0.01$ , \*\*\* $P < 0.001$ .

Figure S2). SCI induced a pronounced increase in anxiety behavior as indicated by reduced time spent in the center of the open field in the two strains of mice. Direct comparisons revealed no significant difference in anxiety behavior between Swiss Webster and C57BL/6 mice after complete transection of the spinal cord (Supplementary Figure S2). Taken together, these data demonstrate that Swiss Webster show better anxiety-independent increase in mobility than C57BL/6 mice after complete transection of the spinal cord.

### Swiss Webster Show Differential Forelimb Gross Sensory Response After Spinal Cord Transection

Next, to investigate possible modification in mouse forelimb sensory tactile response after spinal cord transection, we used open field consisting of sandpapers with low (smooth) and high (rough) granularities, as described previously (Wetzel et al., 2007). C57BL/6 mice showed preference for the rough sandpaper whilst Swiss Webster mice displayed preference for

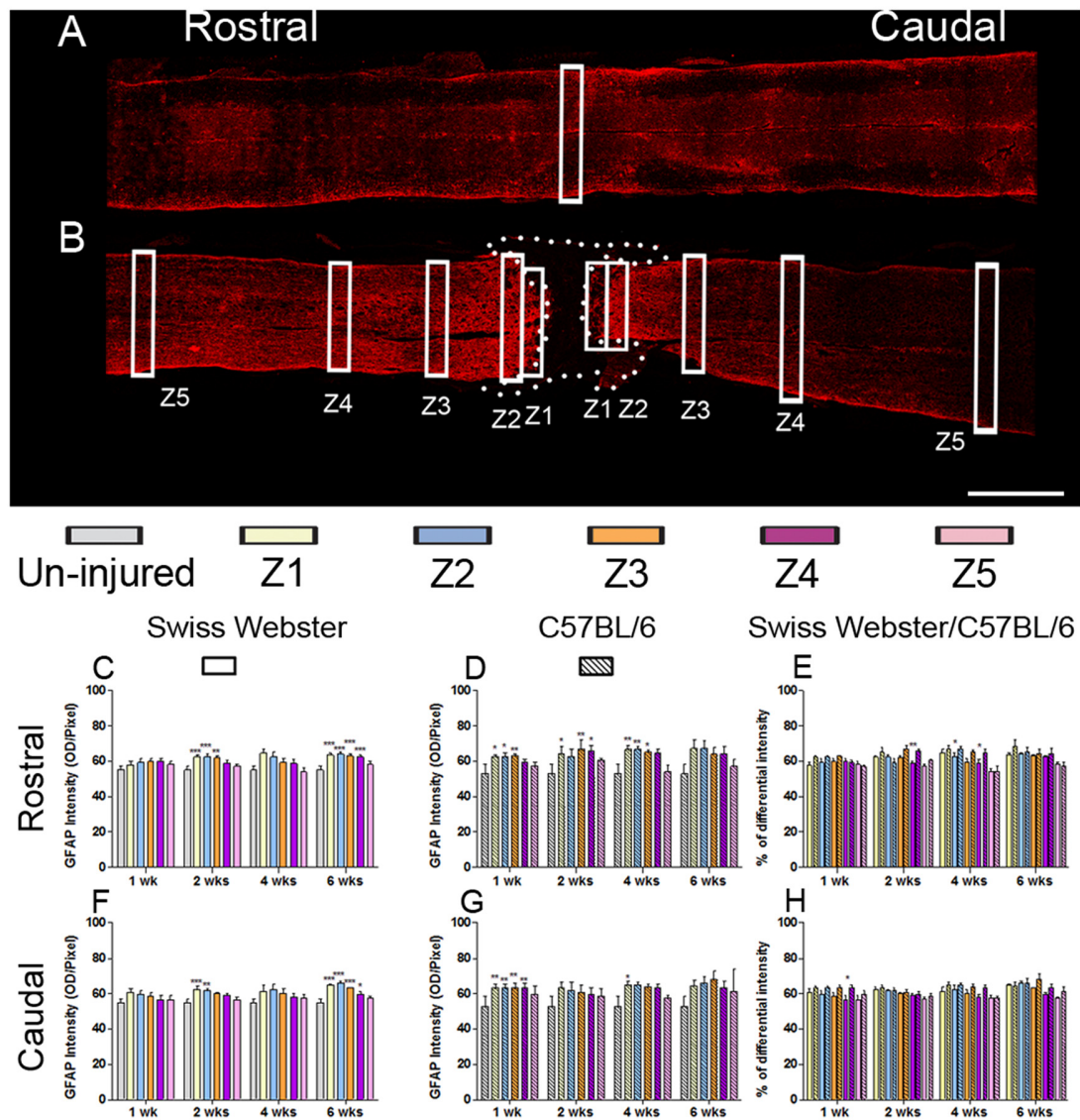


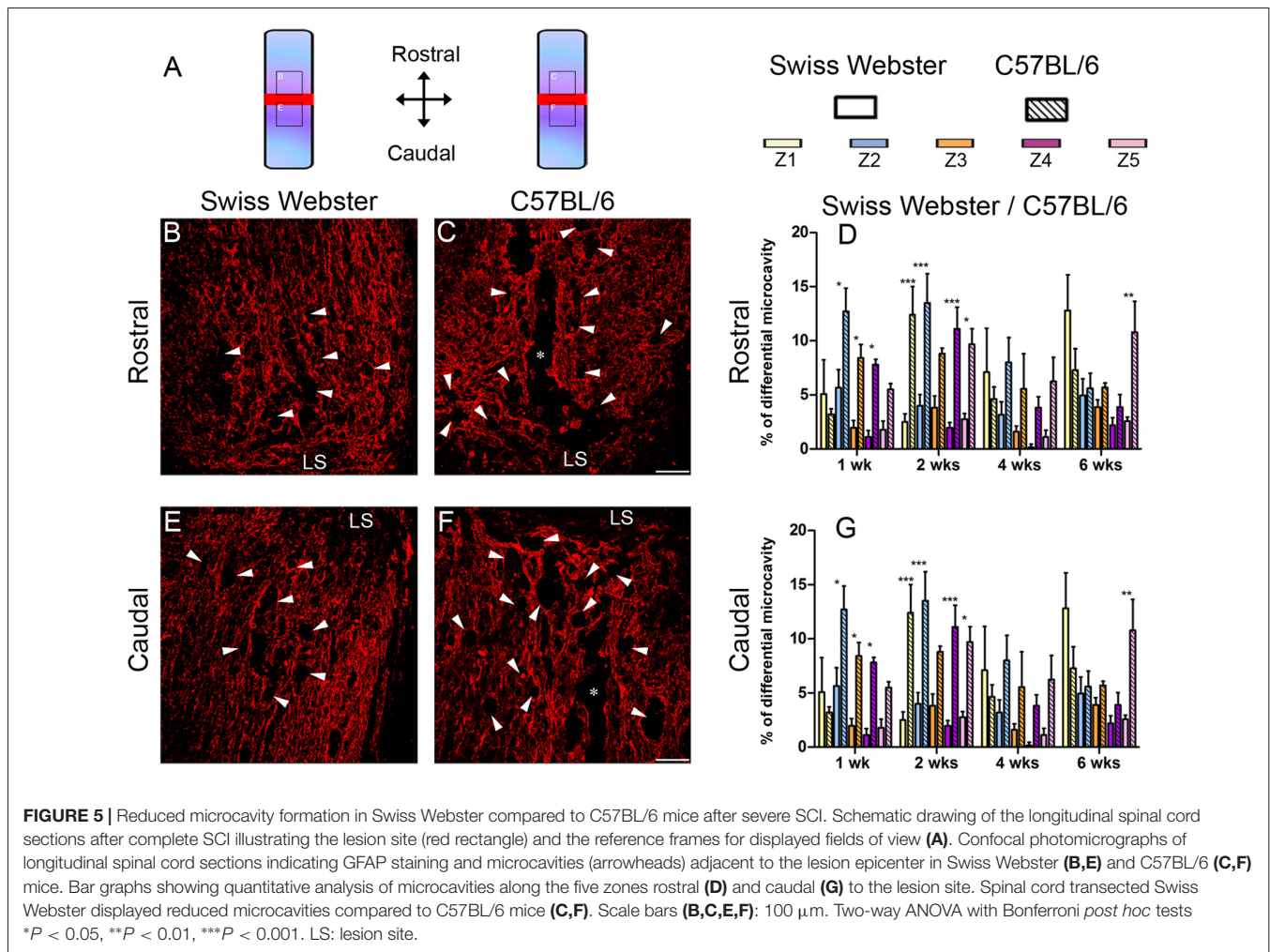
**FIGURE 4 |** Astroglial staining in Swiss Webster and C57BL/6 after severe SCI. Confocal photomicrographs indicating GFAP staining of longitudinal spinal cord sections in the NI control and spinal cord transected mice (A,B). Bar graphs indicating quantitative analysis of GFAP immunoreactivity along the five zones rostral and caudal to the lesion site in Swiss Webster mice (C,F) and C57BL/6 mice (D,G). Direct comparisons revealed that C57BL/6 mice displayed moderate increase in GFAP immunoreactivity compared to Swiss Webster after complete transection of the spinal cord (E,H). Scale bars (A,B): 1 mm. One-way ANOVA with Tukey *post hoc* tests (C,D,F,G) and two-way ANOVA with Bonferroni *post hoc* (E,H). \* $P < 0.05$ , \*\* $P < 0.01$ , \*\*\* $P < 0.001$ .

the smooth sandpaper, as reflected by increase in time spent in these areas of the open field (Figures 2E,F,G,I). Such minor preferences for the rough and smooth sandpapers were evident early after lesion and did not show significant difference compared to before injury (Figures 2G,I). However, direct comparison between the two strains of mice revealed significant differences in their preference between the rough and smooth sandpapers at 24 and 72 h post-lesion (Figures 2H,J). Altogether, tests using sandpapers with different granularities demonstrated differential forelimb gross sensory response between Swiss

Webster and C57BL/6 mice after complete transection of the spinal cord.

### Swiss Webster Display Increased Gliosis Than C57BL/6 Mice After Severe SCI

To examine the potential correlation between increased mobility and glial cell reactivity after severe SCI, we next analyzed microglia/macrophage and astrocyte reactivity between Swiss Webster and C57BL/6 mice following complete transection of the spinal cord. We quantified IBA1 and GFAP intensities and



area fraction in five different zones located at specific distances away from the edge of the astroglia scar border including: (Z1) 0–250  $\mu$ m immediately adjacent to the lesion site, (Z2) between 250–500  $\mu$ m away, (Z3) 1000–1250  $\mu$ m away, (Z4) 2000–2500  $\mu$ m away and (Z5) 4000–4250  $\mu$ m from the lesion site, as previously described (Wanner et al., 2013; see also Figures 3, 4 and Supplementary Figure S1A). In general, gliosis was similar between rostral and caudal to the lesion site in both strains of mice (Figure 3; Swiss Webster Figures 3C,F and C57BL/6 Figures 3D,G). Increased gliosis was more evident within Z1–Z3 compared to more distal regions (Figures 3, 4).

Specifically, Swiss Webster displayed a widespread increase in IBA1 intensity on both sides of the lesion expanding up to zone two that was evident till 6 weeks after injury (Figures 3C,F). C57BL/6 mice, on the other hand, displayed a limited increase in IBA1 intensity only in Z1 at 2 weeks after traumatism rostral and caudal to the lesion site (Figures 3D,G). Comparisons between the two strains of mice revealed a clear increase in IBA1 intensity in Swiss Webster compared to C57BL/6 mice after spinal cord transection (Figures 3E,H). Analysis of area fraction stained with IBA1 further confirmed a higher activation of

macrophage/microglia in the Swiss Webster strain as compared to C57BL/6 (Supplementary Figures S3A–F).

GFAP expression in Swiss Webster mice was increased on both sides of the lesion (Z1–Z3) at 2 and 6 weeks post-injury (Figures 4C,F), whereas in C57BL/6 mice GFAP expression was increased up to 4 weeks post-injury in Z1–Z3 rostral to the lesion site and only up to 1 week after traumatism caudal to the injury site (Figures 4D,G). Direct comparison between the two strains revealed brief increase in GFAP intensity in C57BL/6 up to 4 weeks rostral to the lesion site (Figures 4E,H) as compared to Swiss Webster. However, analysis of area fraction stained with GFAP identified a moderate increase in astrocyte in Swiss Webster as compared to C57BL/6 strain caudal to the lesion (Supplementary Figure S3L). Swiss Webster mice displayed increase in GFAP area fraction rostro-caudal to the lesion site up to 6 weeks post-lesion, whereas C57BL/6 mice showed no changes in GFAP area fraction caudal to the lesion (Supplementary Figures S3G–K). Within the lesion site, an equal astroglia was observed in Swiss Webster and C57BL/6 mice using vimentin (another classical astrocytic marker; Supplementary Figure S4). Altogether, these data demonstrate pronounced microglia/macrophage reactivity as



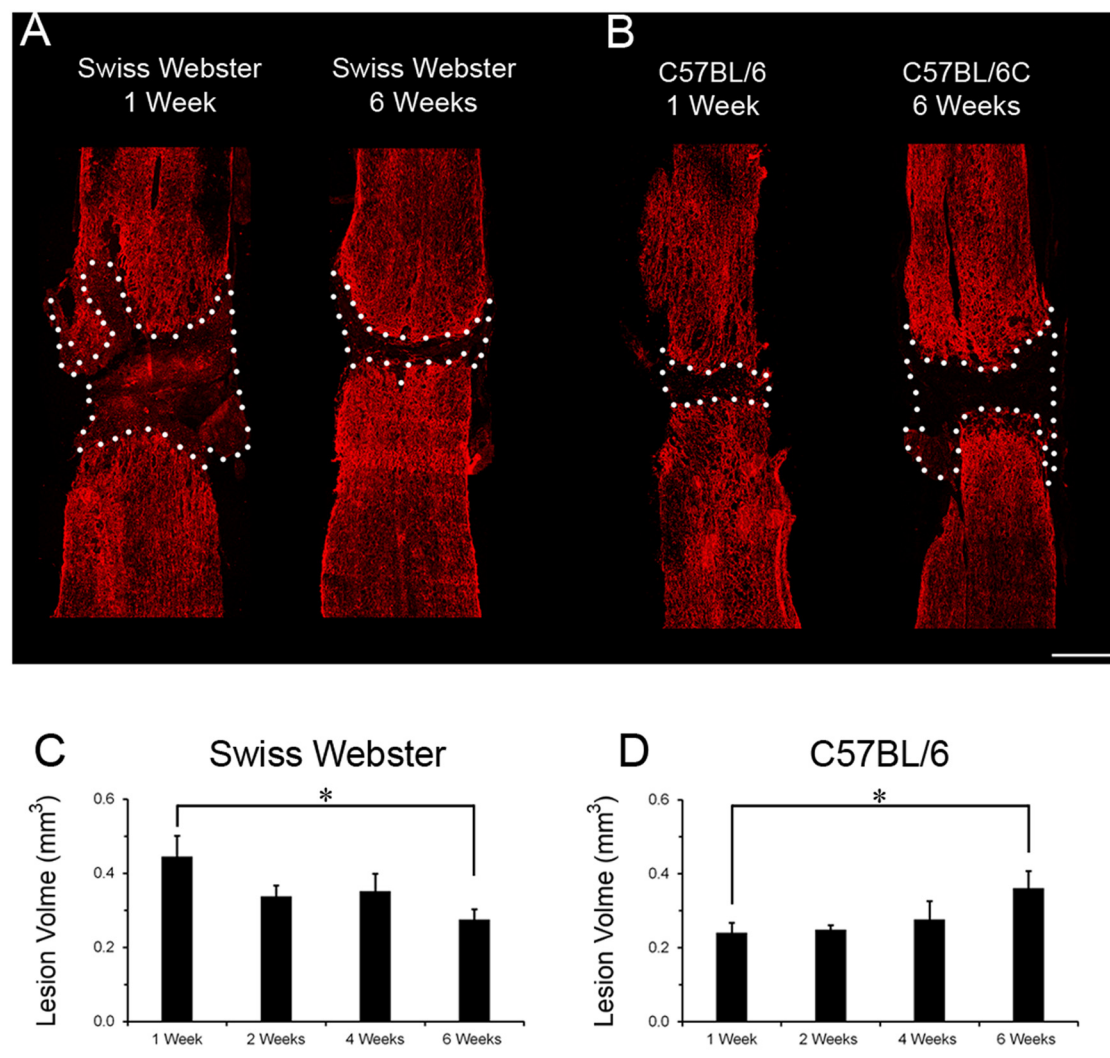


**FIGURE 6 |** Lesion volume evolution in Swiss Webster and C57BL/6 after severe SCI. Confocal photomicrographs indicating GFAP staining and lesion volume evolution (dotted area) in Swiss Webster and C57BL/6 mice (**A,B**) following complete transection of the spinal cord. Bar graphs showing quantitative analysis of lesion volume evolution over-time in Swiss Webster and C57BL/6 mice after complete SCI (**C,D**). Swiss Webster displayed time-dependent decrease, whereas C57BL/6 mice showed increased lesion volume between 1 and 6 weeks after complete transection of the spinal cord (**C,D**). Scale bars (**A,B**): 500  $\mu$ m. Un-paired *t*-test \**P* < 0.05 compared to the same strain at 1 week after injury.

well a moderately increased astrogliosis in Swiss Webster compared to C57BL/6 mice after spinal cord transection.

### Swiss Webster Show Reduced Microcavity and Lesion Volume Than C57BL/6 Mice After Spinal Cord Transection

Finally, to examine the relation between strain-dependent differences in gliosis and tissue preservation after severe SCI, we measured the differences in microcavity formation and lesion volume in Swiss Webster and C57BL/6 mice after complete transection of the spinal cord. Microcavities were measured in the five zones (Z1–Z5) both rostral and caudal to the lesion site (Figure 5). In general, microcavities were

mostly located within Z1 and Z2 (Figures 5B–F). In both strains, microcavities appeared from 1 week and persisted until 6 weeks following injury. NI animals showed no microcavity (data not shown). Direct comparisons between the two strains of mice revealed significantly reduced microcavities in Swiss Webster compared to C57BL/6 mice after spinal cord transection (Figures 5D,G). Reduced microcavities in Swiss Webster compared to C57BL/6 were evident both rostral and caudal to the injury site and reached significance at 1, 2 and 6 weeks following lesion (Figures 5D,G). Lastly, we measured differences in lesion volume evolution after complete transection of the spinal cord between Swiss Webster and C57BL/6 mice (Figure 6). Quantification of the lesion volume based on GFAP delineation revealed time-dependent reduction in Swiss

Webster with significantly decrease between 1 and 6 weeks post-injury (Figures 6A,C). Conversely, C57BL/6 mice displayed time-dependent increase in lesion volume that also reached significance between 1 and 6 weeks after injury (Figures 6B,D). Taken together, these data demonstrate that Swiss Webster mice display reduced microcavity formation and lesion volume than C57BL/6 mice after severe SCI.

## DISCUSSION

In the present study, we carried out detailed behavioral and histopathological analyses after severe SCI in two strains of mice (Swiss Webster and C57BL/6, respectively). Swiss Webster mice displayed increased mobility and differential gross sensory response of their forelimbs following complete transection of the spinal cord than C57BL/6 mice. This behavioral differences post-SCI were associated with enhanced gliosis, reduced microcavity formation and smaller lesion volume. These findings demonstrate strain-dependent differences in behavior after severe SCI that coincides with increased gliosis and preserved histopathology.

### Strain-Dependent Differences in Functional Recovery After SCI

We demonstrate that increased mobility in mice with Swiss Webster genetic background as compared to C57BL/6 mice after complete transection of the spinal cord is associated with increased gliosis, reduced microcavity formation and smaller lesion volume. Others also reported strain-dependent differences in neuroinflammation, tissue preservation and spontaneous functional recovery after incomplete SCI (Basso et al., 2006; Lapointe et al., 2006; Kerr and David, 2007). Inter-strain differences in SCI-induced microglia/macrophages reactivity and neuroinflammation had been reported between C57BL/6, BALB/c and 129X1/SvJ mice after contusion SCI (Ma et al., 2004; Kigerl et al., 2006). However, contrary to our findings, Kigerl et al. (2006) found no consistent correlation between SCI-induced microglia/macrophage activation and lesion size/length in C57BL/6, C57BL/10, BALB/c and B10.PL strains of mice. In fact, the author reported a positive association between increased microglia/macrophage activation and enlarged lesion size only in C57BL/6 mouse strain. Similarly, Ma et al. (2004) had shown that reduced inflammation in 129X1-SvJ mice coincides with increased regeneration compared to C57BL/6 mice after SCI. Divergent to the present study, the two earlier reports applied contusion SCI model that may explain these disparate findings. Previous studies highlight different molecular response including blood-spinal cord barrier (BSCB) leakage between complete transection and other SCI models. Complete transection of the spinal cord at T10 level in institute of cancer research (ICR) strain of mice caused restricted disruption of BSCB than compression SCI, which spread up to cervical level (Pan and Kastin, 2001). In addition, BSCB leakage was only evident within 24 h after complete transection, whereas compression SCI induced a prolonged leakage up to at least 5 days post-lesion (Pan and Kastin, 2001). Another study in C57BL/6 mouse strain also revealed widespread BSCB leakage up

to 6 mm rostro-caudal to the lesion that persisted up to 2 weeks after T8 contusion SCI (Whetstone et al., 2003). Altogether, these findings suggest that complete transection mouse model of SCI induces restricted and a relatively short-term BSCB disruption compared to compression and contusion injuries. This in turn limits tissue oedema, neutrophil infiltration, neuroinflammation and subsequent functional outcome after SCI. Although complete transection of the spinal cord is the most deleterious SCI model, it has several advantages including high reproducibility and reduced inter-individual variations in lesion severity (Lee and Lee, 2013; M'Dahoma et al., 2014). Our result provides the first positive correlation between increased mobility and elevated gliosis after complete transection of the spinal cord in Swiss Webster compared to C57BL/6 mice.

### Reactive Microglia After SCI

Microglia, the native immune occupants of the central nervous system (CNS), are the first responsive glial population after SCI (Tian et al., 2007). Activated microglia have a dual role in SCI pathophysiology. In one hand, increased microglial activation promotes inflammation and tissue damage after SCI (David and Kroner, 2011), whilst on the other hand, they express neurotrophic factors (Lalancette-Hébert et al., 2007; Lambertsen et al., 2009) that promote regeneration following SCI (Mukaino et al., 2010). Transplantation of activated microglia/macrophages into the lesion site promotes axonal regeneration in rats after both incomplete (Prewitt et al., 1997; Rabchevsky and Streit, 1997) and complete SCI (Rapalino et al., 1998). In the latter, axonal re-growth was also associated with partial hind limb motor recovery. Microglia/macrophages activation via pre-incubation with lipopolysaccharide favors expression of neurotrophic factors resulting in reduced microcavity formation and improved functional recovery in rats after SCI (Guth et al., 1994; Hashimoto et al., 2005; Hayakawa et al., 2014). Contrary, several reports have shown that treatment with anti-inflammatory agents including methylprednisolone or interleukin 10 reduce microcavity formation and lesion volume associated with improved functional recovery in rats after incomplete SCI (Bethua et al., 1999; Brewer et al., 1999; Takami et al., 2002). Using cell-specific RNA-sequencing, we have recently demonstrated that microglia/macrophages response exclusively depends on time post-SCI, irrespective of lesion severity (Noristani et al., 2017b). Specifically, early after SCI microglia/macrophages proliferate followed by their prominent role in orchestrating neuroinflammation at more chronic stages after both moderate and severe SCI (Noristani et al., 2017b). Interestingly, we have also recently demonstrated differential morphological changes in microglia/macrophages rostro-caudal to the lesion site following complete transection of the spinal cord in mice with C57BL/6 genetic background (Noristani et al., 2017a). Future studies to analyze strain-dependent differences in microglia/macrophages molecular response after SCI awaits further investigations.

### Reactive Astrocytes After SCI

Cavities and necrotic lesion areas are devoid of reactive astrocytes and are commonly observed in both SCI patients and animal

models. Earlier qualitative studies reported elevated GFAP immunoreactivity in 129X1-SvJ compared to C57BL/6 mice after contusion SCI (Ma et al., 2004; Dixon et al., 2012), although no differences in functional recovery were found between the two strains of mice (Ma et al., 2004). Our finding of increased astrogliosis after complete SCI, even if limited as compared to microglia/macrophage reactivity, suggest that increased astrocytic scar formation may contribute to limiting cavity formation and lesion expansion in Swiss Webster as compared to C57BL/6 mice. Our data are in line with other studies suggesting the positive role of reactive astrocytes after SCI including reduced microcavity formation (Faulkner et al., 2004), isolation of lesion-associated inflammation (Wanner et al., 2013) and expression of pro-regenerative factors (Anderson et al., 2016). In contrast, other reports suggest a detrimental role of astrogliosis following SCI (Menet et al., 2003; Do Thi et al., 2004; Desclaux et al., 2015; Hara et al., 2017). Recently, using cell-specific RNA-sequencing we have demonstrated that astrocyte response after SCI in Swiss Webster mice depends on both time after injury and lesion severity (Noristani and Perrin, 2016; Noristani et al., 2016). Further studies on molecular response of astrocytes between different strains of mice are necessary to uncover the precise mechanisms responsible for improved functional recovery following SCI.

### Increased Gliosis as a Protective Mechanism After Severe SCI

Our findings suggest that increased mobility correlates with increased gliosis, reduced microcavity formation and smaller lesion volume in Swiss Webster than C57BL/6 mice after complete SCI. It is important to note that increased mobility was due to greater use of front paws since we observed no movement of the hind limbs in either Swiss Webster or C57BL/6 mice throughout 6 weeks analyses. Equally important, all mice showed complete anesthesia in their dermatomes caudal to the injury. Our assessment of gross sensory response using sandpapers with different granularities is primarily due to sensation in the forelimbs. This suggests that the increased mobility coincides with local changes in the spinal cord, rather than possible regrowth and reconnection of few descending spinal tracts across the lesion site. In particular, reduced microcavities and smaller lesion volume in Swiss Webster mice are likely to have contributed to the increased mobility. Interestingly, an earlier report in rats with complete transection of the spinal cord had demonstrated that physical exercise prevents regressive changes in the motor neurons and dendrites (Gazula et al., 2004). Given the increased mobility in Swiss Webster, such augmented exercise may also participate in better tissue preservation than C57BL/6 mice after severe SCI. Further studies are required to uncover the specific basis for the increased mobility in Swiss Webster mice after complete transection of the spinal cord.

### CONCLUSION

In conclusion, Swiss Webster and C57BL/6 mice were subjected to complete spinal cord transection to study mobility, gliosis and secondary damages after severe SCI in two strains of mice.

Increased mobility was observed in Swiss Webster that coincides with increased gliosis, reduced microcavity formation and condensed lesion volume compared to C57BL/6 after complete SCI. Uncovering the molecular mechanisms responsible for glial protection may provide novel therapeutic strategies to minimize secondary damages after severe SCI.

### AUTHOR CONTRIBUTIONS

HNN conceptualized the research, designed the project, performed majority of the experiments, analyzed the data and contributed to the writing of the manuscript. LT participated in histological experiments and analysis. FEP conceptualized the research, designed the project, participated in the analysis and data interpretation, drafted the work and gave final approval.

### FUNDING

This work was supported by the patient organizations “Demain Debout Aquitaine” [to HNN and LT] and “Verticale” [to FEP and HNN]. The funding sources were not involved in study design, collection, analysis and interpretation of data as well as in the writing of the report and in the decision to submit the article for publication.

### ACKNOWLEDGMENTS

We thank A. Privat for constructive discussion. We also thank P. Villette, InnovationNet, for the design of the automated softwares (CatMerge and EthoTrack) for CatWalk™ and open field analysis.

### SUPPLEMENTARY MATERIAL

The Supplementary Material for this article can be found online at: <https://www.frontiersin.org/articles/10.3389/fncel.2018.00173/full#supplementary-material>

**FIGURE S1** | Schematic drawing of the longitudinal spinal cord sections from non-injured (NI) control and after complete spinal cord injury (SCI) illustrating the lesion site (red rectangle) and five zones (Z1–Z5) of 250 μm width used for measuring glial reactivity **(A)**. Photomicrographs indicating the experimental arrangement of open field and sandpaper tests used to measure average speed and sensory response after SCI, respectively **(B)**. Photomicrographs displaying example of a full step cycle in NI control **(C)** and spinal cord transected mice **(D)**. Note that no movement of the hind paws were noted in either Swiss Webster or C57BL/6 mice after complete transection of the spinal cord throughout 6 weeks post-injury.

**FIGURE S2** | Swiss Webster and C57BL/6 mice display similar anxiety behavior after spinal cord transection. Bar graphs displaying alterations in anxiety behavior after complete transection of the spinal cord in Swiss Webster **(A)** and C57BL/6 mice **(B)**. Both Swiss Webster and C57BL/6 mice displayed similar increase in anxiety behavior after SCI throughout 6 weeks analysis. One-way ANOVA with Tukey *post hoc* tests. \*\*\* $P < 0.001$  compared to before surgery.

**FIGURE S3** | Differential glial response in Swiss Webster and C57BL/6 mice after severe SCI. Bar graphs indicating quantitative analysis of IBA1 area fraction along the five zones rostral and caudal to the lesion site in Swiss Webster **(A,D)** and C57BL/6 mice **(B,E)**. Direct comparisons revealed that spinal cord transected

Swiss Webster displayed increased IBA1 area fraction compared to C57BL/6 mice both rostral and caudal to the lesion site (C,F). Bar graphs indicating quantitative analysis of GFAP area fraction along the five zones rostral and caudal to the lesion site in Swiss Webster (G,J) and C57BL/6 mice (H,K). Direct comparison showed that transected Swiss Webster displayed moderate increase in GFAP area fraction compared to C57BL/6 caudal to the lesion site (L). One-way ANOVA with Tukey *post hoc* tests (A,B,D,E,G,H,J,K) and two-way ANOVA with Bonferroni *post hoc* (C,F,I,L). \* $P < 0.05$ , \*\* $P < 0.01$ , \*\*\* $P < 0.001$ .

## REFERENCES

- Anderson, M. A., Burda, J. E., Ren, Y., Ao, Y., O'Shea, T. M., Kawaguchi, R., et al. (2016). Astrocyte scar formation aids central nervous system axon regeneration. *Nature* 532, 195–200. doi: 10.1038/nature17623
- Antri, M., Barthe, J. Y., Mouffle, C., and Orsal, D. (2005). Long-lasting recovery of locomotor function in chronic spinal rat following chronic combined pharmacological stimulation of serotonergic receptors with 8-OHDPAT and quipazine. *Neurosci. Lett.* 384, 162–167. doi: 10.1016/j.neulet.2005.04.062
- Basso, D. M., Beattie, M. S., and Bresnahan, J. C. (1996a). Graded histological and locomotor outcomes after spinal cord contusion using the NYU weight-drop device versus transection. *Exp. Neurol.* 139, 244–256. doi: 10.1006/exnr.1996.0098
- Basso, D. M., Beattie, M. S., Bresnahan, J. C., Anderson, D. K., Faden, A. I., Gruner, J. A., et al. (1996b). MASCIS evaluation of open field locomotor scores: effects of experience and teamwork on reliability. Multicenter Animal Spinal Cord Injury Study. *J. Neurotrauma* 13, 343–359. doi: 10.1089/neu.1996.13.343
- Basso, D. M., Fisher, L. C., Anderson, A. J., Jakeman, L. B., McTigue, D. M., and Popovich, P. G. (2006). Basso Mouse Scale for locomotion detects differences in recovery after spinal cord injury in five common mouse strains. *J. Neurotrauma* 23, 635–659. doi: 10.1089/neu.2006.23.635
- Bethea, J. R., Nagashima, H., Acosta, M. C., Briceno, C., Gomez, F., Marcillo, A. E., et al. (1999). Systemically administered interleukin-10 reduces tumor necrosis factor- $\alpha$  production and significantly improves functional recovery following traumatic spinal cord injury in rats. *J. Neurotrauma* 16, 851–863. doi: 10.1089/neu.1999.16.851
- Brewer, K. L., Bethea, J. R., and Yeziarski, R. P. (1999). Neuroprotective effects of interleukin-10 following excitotoxic spinal cord injury. *Exp. Neurol.* 159, 484–493. doi: 10.1006/exnr.1999.7173
- Cahoy, J. D., Emery, B., Kaushal, A., Foo, L. C., Zamanian, J. L., Christopherson, K. S., et al. (2008). A transcriptome database for astrocytes, neurons, and oligodendrocytes: a new resource for understanding brain development and function. *J. Neurosci.* 28, 264–278. doi: 10.1523/JNEUROSCI.4178-07.2008
- David, S., and Kroner, A. (2011). Repertoire of microglial and macrophage responses after spinal cord injury. *Nat. Rev. Neurosci.* 12, 388–399. doi: 10.1038/nrn3053
- Desclaux, M., Perrin, F. E., Do-Thi, A., Prieto-Cappellini, M., Gimenez Y Ribotta, M., Mallet, J., et al. (2015). Lentiviral-mediated silencing of glial fibrillary acidic protein and vimentin promotes anatomical plasticity and functional recovery after spinal cord injury. *J. Neurosci. Res.* 93, 43–55. doi: 10.1002/jnr.23468
- Dixon, K. J., Munro, K. M., Boyd, A. W., Bartlett, P. F., and Turnley, A. M. (2012). Partial change in EphA4 knockout mouse phenotype: loss of diminished GFAP upregulation following spinal cord injury. *Neurosci. Lett.* 525, 66–71. doi: 10.1016/j.neulet.2012.07.023
- Do Thi, N. A., Saillour, P., Ferrero, L., Dedieu, J. F., Mallet, J., and Paunio, T. (2004). Delivery of GDNF by an E1,E3/E4 deleted adenoviral vector and driven by a GFAP promoter prevents dopaminergic neuron degeneration in a rat model of Parkinson's disease. *Gene Ther.* 11, 746–756. doi: 10.1038/sj.gt.3302222
- Faulkner, J. R., Herrmann, J. E., Woo, M. J., Tansey, K. E., Doan, N. B., and Sofroniew, M. V. (2004). Reactive astrocytes protect tissue and preserve function after spinal cord injury. *J. Neurosci.* 24, 2143–2155. doi: 10.1523/JNEUROSCI.3547-03.2004
- Gadani, S. P., Walsh, J. T., Smirnov, I., Zheng, J., and Kipnis, J. (2015). The glia-derived alarmin IL-33 orchestrates the immune response and promotes

recovery following CNS injury. *Neuron* 85, 703–709. doi: 10.1016/j.neuron.2015.01.013

Gazula, V. R., Roberts, M., Luzzio, C., Jawad, A. F., and Kalb, R. G. (2004). Effects of limb exercise after spinal cord injury on motor neuron dendrite structure. *J. Comp. Neurol.* 476, 130–145. doi: 10.1002/cne.20204

Gerber, Y. N., Sabourin, J. C., Rabano, M., Vivanco, M., and Perrin, F. E. (2012). Early functional deficit and microglial disturbances in a mouse model of amyotrophic lateral sclerosis. *PLoS One* 7:e36000. doi: 10.1371/journal.pone.0036000

Guth, L., Zhang, Z., DiProspero, N. A., Joubin, K., and Fitch, M. T. (1994). Spinal cord injury in the rat: treatment with bacterial lipopolysaccharide and indomethacin enhances cellular repair and locomotor function. *Exp. Neurol.* 126, 76–87. doi: 10.1006/exnr.1994.1043

Hara, M., Kobayakawa, K., Ohkawa, Y., Kumamaru, H., Yokota, K., Saito, T., et al. (2017). Interaction of reactive astrocytes with type I collagen induces astrocytic scar formation through the integrin-N-cadherin pathway after spinal cord injury. *Nat. Med.* 23, 818–828. doi: 10.1038/nm.4354

Hashimoto, M., Nitta, A., Fukumitsu, H., Nomoto, H., Shen, L., and Furukawa, S. (2005). Inflammation-induced GDNF improves locomotor function after spinal cord injury. *Neuroreport* 16, 99–102. doi: 10.1097/00001756-200502080-00004

Hausmann, O. N. (2003). Post-traumatic inflammation following spinal cord injury. *Spinal Cord* 41, 369–378. doi: 10.1038/sj.sc.3101483

Hayakawa, K., Okazaki, R., Morioka, K., Nakamura, K., Tanaka, S., and Ogata, T. (2014). Lipopolysaccharide preconditioning facilitates M2 activation of resident microglia after spinal cord injury. *J. Neurosci. Res.* 92, 1647–1658. doi: 10.1002/jnr.23448

Hirasawa, T., Ohsawa, K., Imai, Y., Ondo, Y., Akazawa, C., Uchino, S., et al. (2005). Visualization of microglia in living tissues using Iba1-EGFP transgenic mice. *J. Neurosci. Res.* 81, 357–362. doi: 10.1002/jnr.20480

Hirbec, H., Marmai, C., Duroux-Richard, I., Roubert, C., Esclangon, A., Croze, S., et al. (2018). The microglial reaction signature revealed by RNAseq from individual mice. *Glia* 66, 971–986. doi: 10.1002/glia.23295

Kerr, B. J., and David, S. (2007). Pain behaviors after spinal cord contusion injury in two commonly used mouse strains. *Exp. Neurol.* 206, 240–247. doi: 10.1016/j.expneurol.2007.04.014

Kigerl, K. A., McLaughly, V. M., and Popovich, P. G. (2006). Comparative analysis of lesion development and intraspinal inflammation in four strains of mice following spinal contusion injury. *J. Comp. Neurol.* 494, 578–594. doi: 10.1002/cne.20827

Lalancette-Hébert, M., Gowing, G., Simard, A., Weng, Y. C., and Kriz, J. (2007). Selective ablation of proliferating microglial cells exacerbates ischemic injury in the brain. *J. Neurosci.* 27, 2596–2605. doi: 10.1523/JNEUROSCI.5360-06.2007

Lambertsen, K. L., Clausen, B. H., Babcock, A. A., Gregersen, R., Fenger, C., Nielsen, H. H., et al. (2009). Microglia protect neurons against ischemia by synthesis of tumor necrosis factor. *J. Neurosci.* 29, 1319–1330. doi: 10.1523/JNEUROSCI.5505-08.2009

Lapointe, N. P., Ung, R. V., Bergeron, M., Cote, M., and Guertin, P. A. (2006). Strain-dependent recovery of spontaneous hindlimb movement in spinal cord transected mice (CD1, C57BL/6, BALB/c). *Behav. Neurosci.* 120, 826–834. doi: 10.1037/0735-7044.120.4.826

Lee, D. H., and Lee, J. K. (2013). Animal models of axon regeneration after spinal cord injury. *Neurosci. Bull.* 29, 436–444. doi: 10.1007/s12264-013-1365-4

Ma, M., Wei, P., Wei, T., Ransohoff, R. M., and Jakeman, L. B. (2004). Enhanced axonal growth into a spinal cord contusion injury site in a strain of mouse (129X1/SvJ) with a diminished inflammatory response. *J. Comp. Neurol.* 474, 469–486. doi: 10.1002/cne.20149

- M'Dahoma, S., Bourgoïn, S., Kayser, V., Barthélemy, S., Chevarin, C., Chali, F., et al. (2014). Spinal cord transection-induced allodynia in rats—behavioral, physiopathological and pharmacological characterization. *PLoS One* 9:e102027. doi: 10.1371/journal.pone.0102027
- Menet, V., Prieto, M., Privat, A., and Giménez Y Ribotta, M. (2003). Axonal plasticity and functional recovery after spinal cord injury in mice deficient in both glial fibrillary acidic protein and vimentin genes. *Proc. Natl. Acad. Sci. U S A* 100, 8999–9004. doi: 10.1073/pnas.1533187100
- Mukaino, M., Nakamura, M., Yamada, O., Okada, S., Morikawa, S., Renault-Mihara, F., et al. (2010). Anti-IL-6-receptor antibody promotes repair of spinal cord injury by inducing microglia-dominant inflammation. *Exp. Neurol.* 224, 403–414. doi: 10.1016/j.expneurol.2010.04.020
- Nelissen, S., Vanganswinkel, T., Geurts, N., Geboes, L., Lemmens, E., Vidal, P. M., et al. (2014). Mast cells protect from post-traumatic spinal cord damage in mice by degrading inflammation-associated cytokines via mouse mast cell protease 4. *Neurobiol. Dis.* 62, 260–272. doi: 10.1016/j.nbd.2013.09.012
- Noristani, H. N., Boukhaddaoui, H., Saint-Martin, G., Auzer, P., Sidiboulenouar, R., Lonjon, N., et al. (2017a). A combination of *Ex vivo* diffusion MRI and multiphoton to study microglia/monocytes alterations after spinal cord injury. *Front. Aging Neurosci.* 9:230. doi: 10.3389/fnagi.2017.00230
- Noristani, H. N., Gerber, Y. N., Sabourin, J.-C., Le Corre, M., Lonjon, N., Mestre-Frances, N., et al. (2017b). RNA-seq analysis of microglia reveals time-dependent activation of specific genetic programs following spinal cord injury. *Front. Mol. Neurosci.* 10:90. doi: 10.3389/fnmol.2017.00090
- Noristani, H. N., Lonjon, N., Cardoso, M., Le Corre, M., Chan-Seng, E., Captier, G., et al. (2015). Correlation of *in vivo* and *ex vivo* <sup>1</sup>H-MRI with histology in two severities of mouse spinal cord injury. *Front. Neuroanat.* 9:24. doi: 10.3389/fnana.2015.00024
- Noristani, H. N., and Perrin, F. E. (2016). Astrocyte-to-neuron conversion induced by spinal cord injury. *Oncotarget* 7, 83831–83832. doi: 10.18632/oncotarget.13780
- Noristani, H. N., Sabourin, J. C., Boukhaddaoui, H., Chan-Seng, E., Gerber, Y. N., and Perrin, F. E. (2016). Spinal cord injury induces astroglial conversion towards neuronal lineage. *Mol. Neurodegener.* 11:68. doi: 10.1186/s13024-016-0133-0
- Onifer, S. M., Rabchevsky, A. G., and Scheff, S. W. (2007). Rat models of traumatic spinal cord injury to assess motor recovery. *ILAR J.* 48, 385–395. doi: 10.1093/ilar.48.4.385
- Pan, W., and Kastin, A. J. (2001). Increase in TNF $\alpha$  transport after SCI is specific for time, region, and type of lesion. *Exp. Neurol.* 170, 357–363. doi: 10.1006/exnr.2001.7702
- Prewitt, C. M., Niesman, I. R., Kane, C. J., and Houllé, J. D. (1997). Activated macrophage/microglial cells can promote the regeneration of sensory axons into the injured spinal cord. *Exp. Neurol.* 148, 433–443. doi: 10.1006/exnr.1997.6694
- Rabchevsky, A. G., and Streit, W. J. (1997). Grafting of cultured microglial cells into the lesioned spinal cord of adult rats enhances neurite outgrowth. *J. Neurosci. Res.* 47, 34–48. doi: 10.1002/(sici)1097-4547(19970101)47:1<34::aid-jnr4>3.3.co;2-1
- Rapalino, O., Lazarov-Spiegler, O., Agranov, E., Velan, G. J., Yoles, E., Fraidakis, M., et al. (1998). Implantation of stimulated homologous macrophages results in partial recovery of paraplegic rats. *Nat. Med.* 4, 814–821. doi: 10.1038/nm0798-814
- Solga, A. C., Pong, W. W., Walker, J., Wylie, T., Magrini, V., Apicelli, A. J., et al. (2015). RNA-sequencing reveals oligodendrocyte and neuronal transcripts in microglia relevant to central nervous system disease. *Glia* 63, 531–548. doi: 10.1002/glia.22754
- Takami, T., Oudega, M., Bethea, J. R., Wood, P. M., Kleitman, N., and Bunge, M. B. (2002). Methylprednisolone and interleukin-10 reduce gray matter damage in the contused Fischer rat thoracic spinal cord but do not improve functional outcome. *J. Neurotrauma* 19, 653–666. doi: 10.1089/089771502753754118
- Thuret, S., Thallmair, M., Horky, L. L., and Gage, F. H. (2012). Enhanced functional recovery in MRL/MpJ mice after spinal cord dorsal hemisection. *PLoS One* 7:e30904. doi: 10.1371/journal.pone.0030904
- Tian, D. S., Dong, Q., Pan, D. J., He, Y., Yu, Z. Y., Xie, M. J., et al. (2007). Attenuation of astrogliosis by suppressing of microglial proliferation with the cell cycle inhibitor olomoucine in rat spinal cord injury model. *Brain Res.* 1154, 206–214. doi: 10.1016/j.brainres.2007.04.005
- van den Berg, M. E., Castellote, J. M., Mahillo-Fernandez, I., and de Pedro-Cuesta, J. (2010). Incidence of spinal cord injury worldwide: a systematic review. *Neuroepidemiology* 34, 184–192; discussion 192. doi: 10.1159/000279335
- Wanner, I. B., Anderson, M. A., Song, B., Levine, J., Fernandez, A., Gray-Thompson, Z., et al. (2013). Glial scar borders are formed by newly proliferated, elongated astrocytes that interact to corral inflammatory and fibrotic cells via STAT3-dependent mechanisms after spinal cord injury. *J. Neurosci.* 33, 12870–12886. doi: 10.1523/JNEUROSCI.2121-13.2013
- Wetzel, C., Hu, J., Riethmacher, D., Benckendorff, A., Harder, L., Eilers, A., et al. (2007). A stomatin-domain protein essential for touch sensation in the mouse. *Nature* 445, 206–209. doi: 10.1038/nature05394
- Whetstone, W. D., Hsu, J. Y., Eisenberg, M., Werb, Z., and Noble-Haeusslein, L. J. (2003). Blood-spinal cord barrier after spinal cord injury: relation to revascularization and wound healing. *J. Neurosci. Res.* 74, 227–239. doi: 10.1002/jnr.10759

**Conflict of Interest Statement:** The authors declare that the research was conducted in the absence of any commercial or financial relationships that could be construed as a potential conflict of interest.

Copyright © 2018 Noristani, They and Perrin. This is an open-access article distributed under the terms of the Creative Commons Attribution License (CC BY). The use, distribution or reproduction in other forums is permitted, provided the original author(s) and the copyright owner are credited and that the original publication in this journal is cited, in accordance with accepted academic practice. No use, distribution or reproduction is permitted which does not comply with these terms.